Supplement of Atmos. Chem. Phys., 25, 14967–14986, 2025 https://doi.org/10.5194/acp-25-14967-2025-supplement © Author(s) 2025. CC BY 4.0 License.





Supplement of

Influence of oceanic ventilation and terrestrial transport on the atmospheric volatile chlorinated hydrocarbons over the Western Pacific

Shan-Shan Liu et al.

Correspondence to: Zhen He (zhenhe@ouc.edu.cn) and Gui-Peng Yang (gpyang@mail.ouc.edu.cn)

The copyright of individual parts of the supplement might differ from the article licence.

S1. Oceanographic characteristics of the Western Pacific

1

2

3

4

5

6

7

8

9

10

11

12

13

14

15

16

17

18

19

20

21

22

23

24

25

In the Western Pacific, the North Equatorial Current (NEC) is a broad westward flow characterized by high temperature, high salinity, high transparency, and low nutrient concentrations. Upon reaching the Philippine coast, the NEC bifurcates into branches: the northward-flowing Kuroshio Current two (KC) and the southward-flowing Mindanao Current (MC). The KC continues northward and, off the east coast of Japan, encounters the low-salinity, nutrient-rich Oyashio Current (OC), forming the Kuroshio-Oyashio Extension (KOE). Meanwhile, the Equatorial Undercurrent flows rapidly eastward, carrying a narrow band of high-salinity, oxygen-rich waters. Based on historical regional classifications and previous literature (Roden, 1991; Nan et al., 2015; Du et al., 2022; Xu et al., 2023), combined with the spatial distributions of seawater temperature, salinity, nutrient concentrations, and Chl-a concentrations observed in this study (Fig. S1 and Fig. S2), the Western Pacific survey area was subdivided into three representative regimes: the KOE, the North Pacific Subtropical Gyre (NPSG), and the Western Pacific Warm Pool (WPWP). In the KOE, pronounced thermal and haline fronts intensify mesoscale eddies and vertical mixing, enhancing nutrient supply to the euphotic zone and stimulating primary production, as reflected by elevated Chl-a concentrations in this region (Fig. S1 and Fig. S2). In contrast, the NPSG exhibits typical oligotrophic conditions, with elevated surface salinity (>34), severe nutrient depletion, and extremely low Chl-a concentrations (Fig. S1 and Fig. S2), earning it the designation of an "ocean desert." The WPWP, extending from 10°S to 10°N, is distinguished by persistently high sea surface temperatures (>29 °C), abundant precipitation, and vigorous air-sea interactions, underscoring its critical role in regulating the global climate system.

However, strong thermal stratification and the presence of a barrier layer suppress nutrient entrainment across the thermocline, thereby constraining phytoplankton growth and resulting in relatively low Chl-a concentrations and primary productivity

29 (Fig. S1 and Fig. S2).

30

31

32

33

34

35

36

37

38

39

40

41

42

43

44

45

46

47

48

49

50

S2. Accuracy of the dynamic dilution system

Calibration curves were established using a 100 ppbv standard mixture gas (Spectra Gases, USA), which was dynamically diluted with ultra-high-purity nitrogen via a mass-flow–controlled dilution system (Nutech 2202A; accuracy $\pm 1\%$) to achieve pptv-low ppbv concentration levels. Six concentration gradients were prepared, and the diluted standards were analyzed following the same procedures as the field samples. The results showed that the correlation coefficients of the calibration curves for all target compounds are ≥ 0.996 , indicating excellent linearity and methodological reliability. To ensure calibration accuracy and international comparability, aliquots of the diluted standard gases were sent to the China Meteorological Administration Meteorological Observation Centre (CMA-MOC) for independent analysis using an AGAGE-traceable Medusa-GC/MS system (Zhang et al., 2017; Yu et al., 2020; An et al., 2021). The CMA-MOC results were reported as dry-air mole fractions on calibration scales established and maintained by the Scripps Institution of Oceanography (SIO) (Prinn et al., 2000; Miller et al., 2008). The intercomparison indicated that the differences between our measurements and those from CMA-MOC for target compounds were within $\pm 5\%$: CHCl₃ (-4.3% to -1.2%), CH₃CCl₃ (+1.5% to

S3. Evaluation indexes in atmospheric VCHCs measurements

+4.6%), and CCl₄ (+1.1% to +3.8%).

Precision was evaluated in accordance with US EPA (2019) guidelines by

conducting seven replicate analyses of standard gas samples prepared at environmentally relevant concentrations. These concentrations reflect typical atmospheric levels of the target VCHCs (CHCl₃, C₂HCl₃, CH₃CCl₃, and CCl₄), as referenced in WMO (2022). The test standards were generated by dynamically diluting a 100 ppbv primary mixture (Spectra Gases, USA) with ultra-high-purity nitrogen using a dynamic dilution system (Nutech 2202A). Under consistent analytical conditions, each standard gas sample was measured seven times. Precision was expressed as the relative standard deviation (RSD, %) calculated using Eq. (S1).

Precision = RSD_(X) =
$$\frac{\sqrt{\frac{\sum_{i=1}^{n} (X_{(i)} - \overline{X})^{2}}{n-1}}}{\overline{X}} \times 100\%$$
 (S1)

where $X_{(i)}$ denotes the measured concentration of the target compound in the sample gas derived from a multipoint external calibration curve. \overline{X} is the arithmetic mean of seven replicate measurements, and n=7. The precision results at ambient-relevant concentrations are summarized in Table S1.

In this study, the method detection limits (MDL) of atmospheric target compounds were determined by the U.S. Environmental Protection Agency (US EPA, 2019) procedure. Specifically, low-concentration standard gases at approximately five times the expected MDL were prepared using a dynamic dilution system, and seven complete analytical runs—including standard gas preparation, preconcentration, injection, chromatographic separation, and mass spectrometric detection—were conducted. MDL was calculated as MDL = $t \times S$, where S is the standard deviation of seven replicate measurements and t is the Student's t-value at the 99% confidence level with six degrees of freedom (3.143). The MDL for each target compound is listed in Table S1.

- **73 Figures: S1-S8**
- 74 Fig. S1. Horizontal distributions of temperature (a), salinity (b), and Chl-a (c) in
- surface seawater of the Western Pacific. (Figures generated using Ocean Data View;
- 76 Schlitzer, Reiner, Ocean Data View, odv.awi.de, 2025).
- 77 Fig. S2. Vertical profiles of temperature, salinity, Chl-a, and nutrients at depths of
- 78 0–200 m in the Western Pacific.(Figures generated using Ocean Data View; Schlitzer,
- 79 Reiner, Ocean Data View, odv.awi.de, 2025).
- Fig. S3. Boxplots showing the atmospheric concentrations of VCHCs at all sampling
- 81 locations during the study period.
- Fig. S4. 96 h back trajectories of air masses over the Western Pacific. The ensemble
- 96 h back-trajectories are within the lower troposphere above 10 m (red lines), above
- 84 100 m (blue lines), and above 1000 m (green lines).
- 85 Fig. S5. Linear correlations between the atmospheric mixing ratios of SF₆ and those
- of CHCl₃ (a) and C₂HCl₃ (b) in the Western Pacific. Solid lines denote the linear
- best-fit curves, and shaded areas represent the 95% confidence intervals.
- 88 **Fig. S6.** Linear correlations between the Chl-a concentration and atmospheric mixing
- ratios of CHCl₃ (a) and C₂HCl₃ (b) in the Western Pacific. Solid lines denote the
- 90 linear best-fit curves, and shaded areas represent the 95% confidence intervals.
- 91 Fig. S7. Relationships between CHCl₃, CCl₄, C₂HCl₃, and CH₃CCl₃ in the atmosphere of
- 92 the Western Pacific.
- 93 Fig. S8. Relationships between CHCl₃, CCl₄, C₂HCl₃, and CH₃CCl₃ in the seawater of
- 94 the Western Pacific.

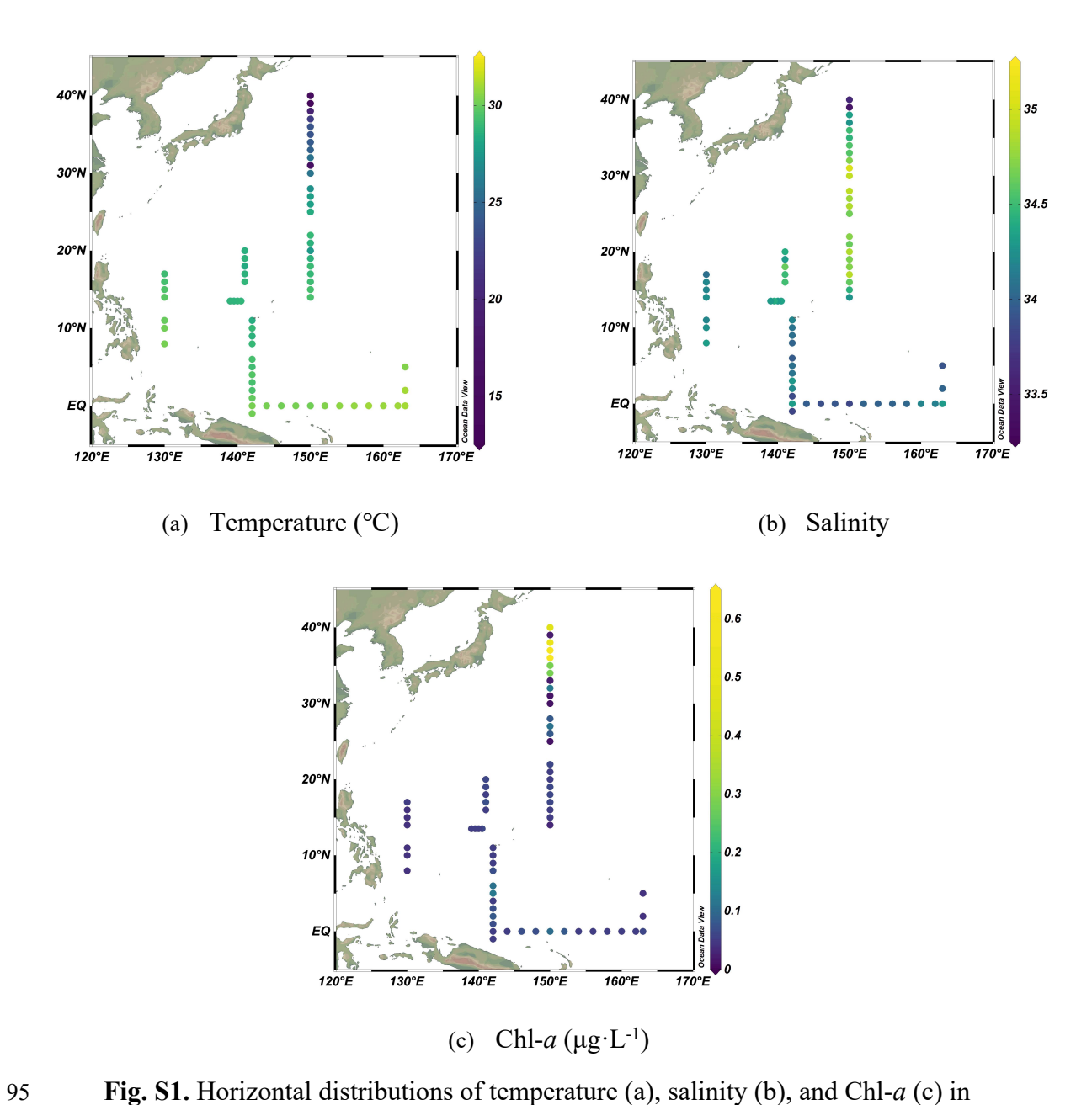


Fig. S1. Horizontal distributions of temperature (a), salinity (b), and Chl-a (c) in surface seawater of the Western Pacific. (Figures generated using Ocean Data View; Schlitzer, Reiner, Ocean Data View, odv.awi.de, 2025).

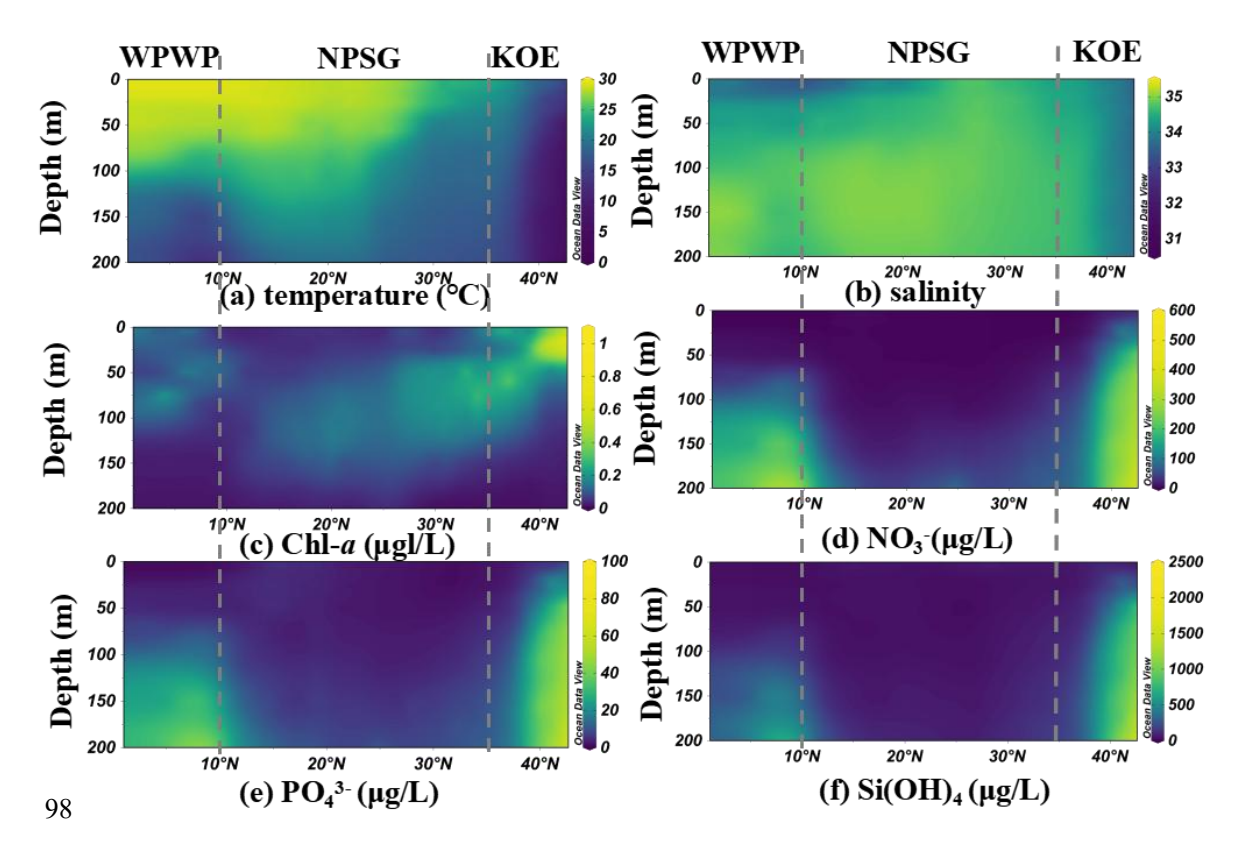


Fig. S2. Vertical profiles of temperature, salinity, Chl-*a*, and nutrients at depths of 0–200 m in the Western Pacific. (Figures generated using Ocean Data View; Schlitzer, Reiner, Ocean Data View, odv.awi.de, 2025).

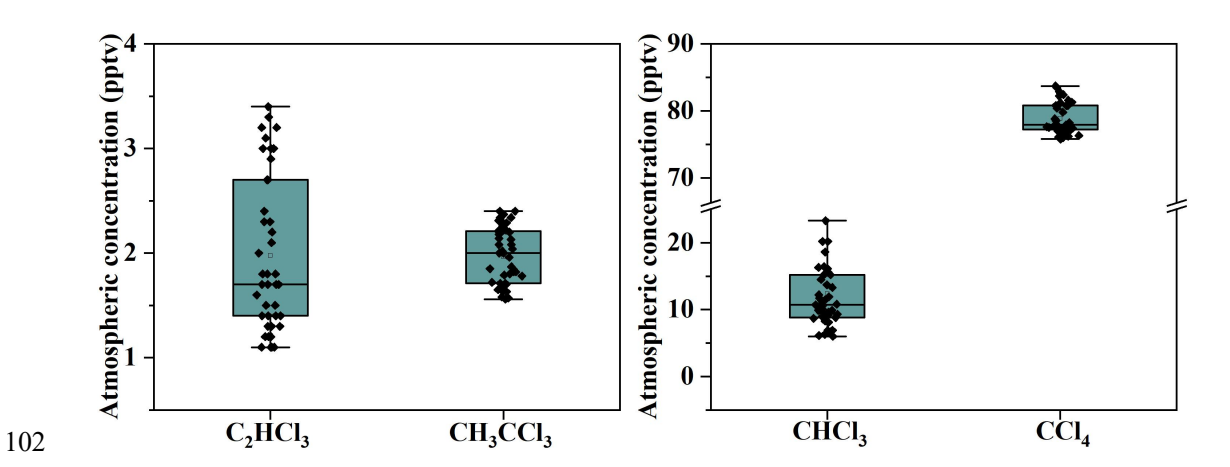


Fig. S3. Boxplots showing the atmospheric concentrations of VCHCs at all sampling locations during the study period.

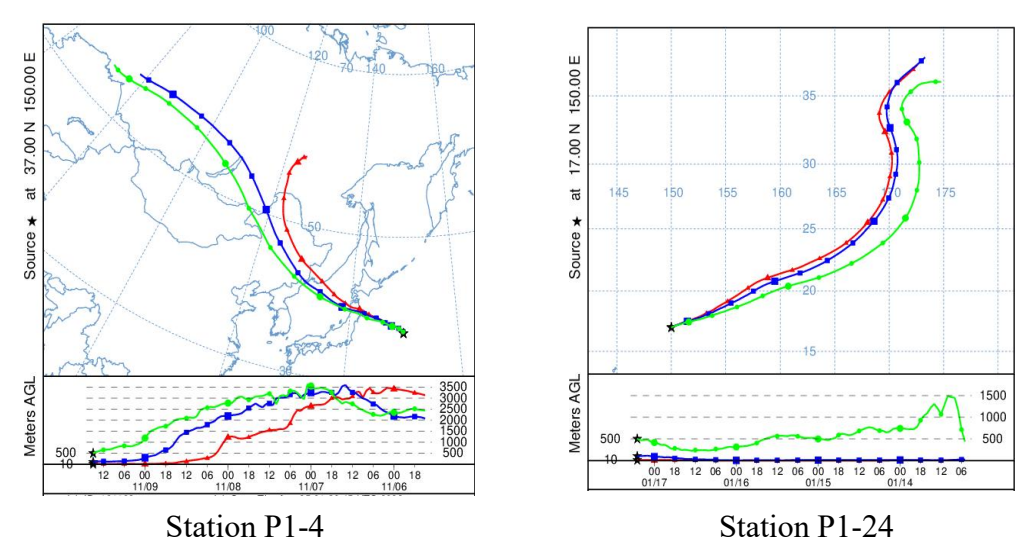


Fig. S4. 96 h back trajectories of air masses over the Western Pacific. The ensemble 96 h back-trajectories are within the lower troposphere above 10 m (red lines), above 100 m (blue lines), and above 1000 m (green lines).

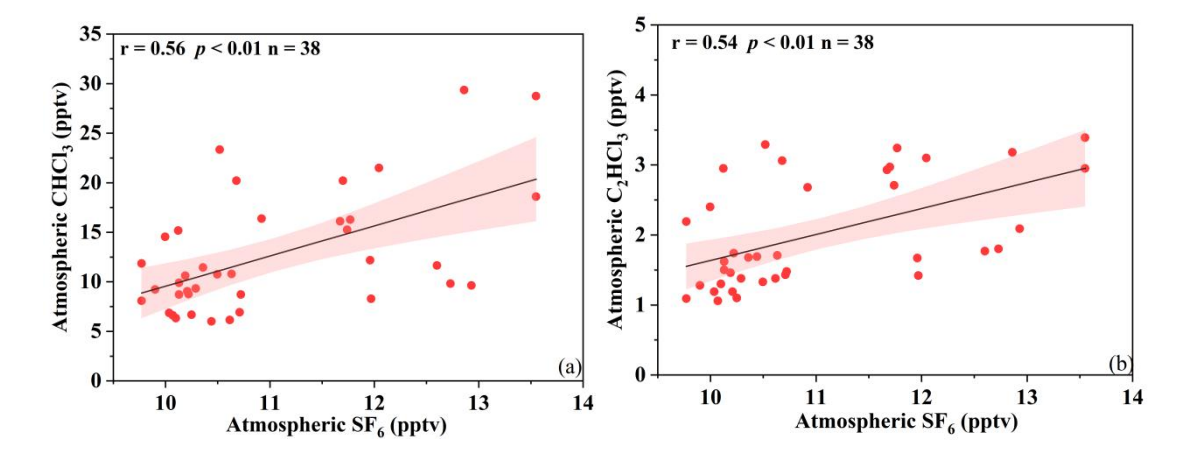


Fig. S5. Linear correlations between the atmospheric mixing ratios of SF₆ and those of CHCl₃ (a) and C₂HCl₃ (b) in the Western Pacific. Solid lines denote the linear best-fit curves, and shaded areas represent the 95% confidence intervals.

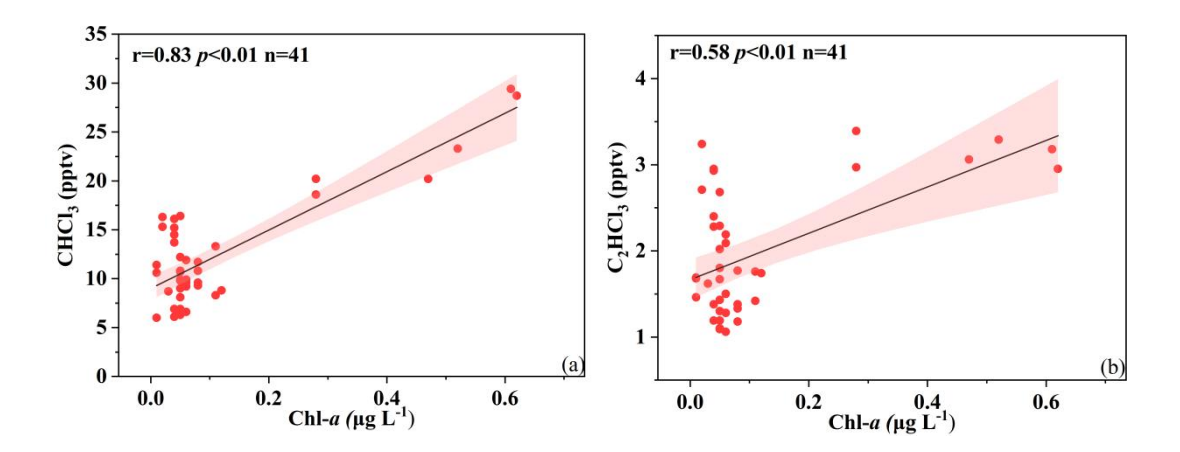


Fig. S6. Linear correlations between the Chl-*a* concentration and atmospheric mixing ratios of CHCl₃ (a) and C₂HCl₃ (b) in the Western Pacific. Solid lines denote the linear best-fit curves, and shaded areas represent the 95% confidence intervals.

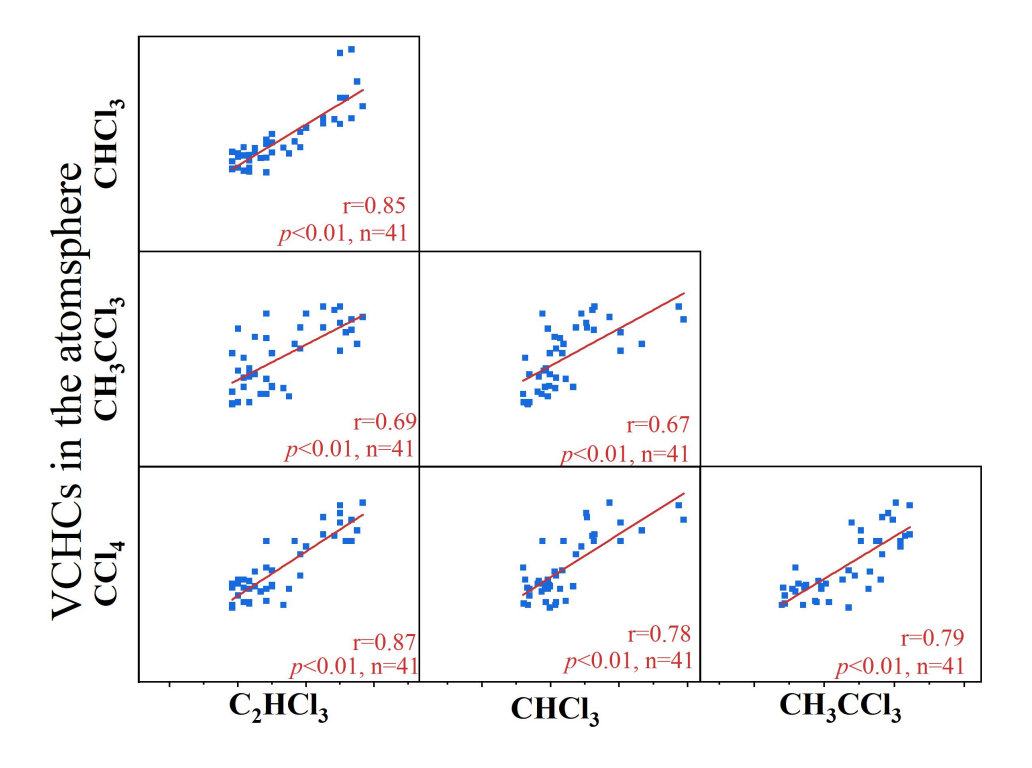


Fig. S7. Relationships between CHCl₃, CCl₄, C₂HCl₃, and CH₃CCl₃ in the atmosphere of the Western Pacific.

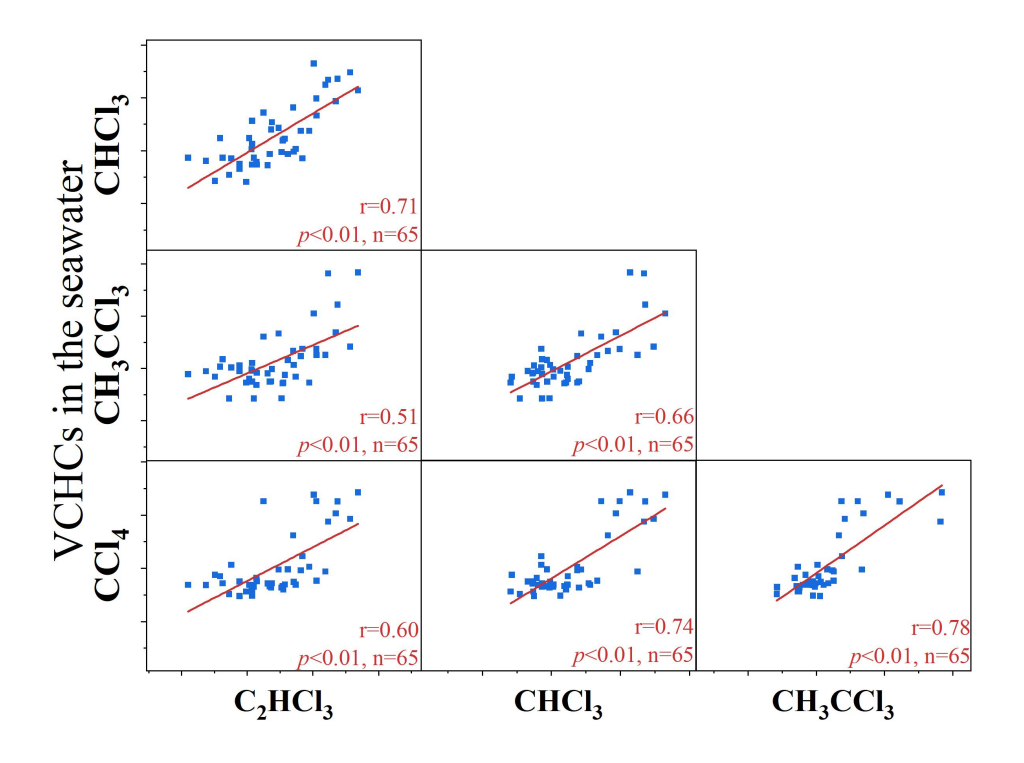


Fig. S8. Relationships between CHCl₃, CCl₄, C₂HCl₃, and CH₃CCl₃ in the seawater of the Western Pacific.

125 **Table: S1**

126

Table S1. The method detection limits (MDL), measurement precision, and atmospheric lifetimes of the selected VCHCs in air.

Compound	Typical ambient concentration	Precision at ambient-relevant concentration ¹	MDL ²	Lifetime ³
	pptv	%RSD, n = 7	pptv	
CHCl ₃	10-15	3.2	0.50	178 days
C_2HCl_3	2-5	4.9	0.10	5.6 days
CH ₃ CCl ₃	2-3	6.3	0.20	5 years
CCl ₄	80-100	1.1	1.00	30 years

- Notes: ¹Precision at ambient-relevant concentrations is expressed as RSD (%), based on
- seven replicate measurements of mixed standard gases: 2 pptv (C₂HCl₃, CH₃CCl₃), 10
- pptv (CHCl₃), and 100 pptv (CCl₄).
- 131 ²MDL refers to the method detection limit as determined in accordance with the US EPA
- 132 procedure (2019).
- ³Atmospheric lifetimes are taken from WMO (2022).

- 134 References
- An, M., Western, L. M., Say, D., Chen, L., Claxton, T., Ganesan, A. L., Hossaini, R.,
- Krummel, P. B., Manning, A. J., and Mühle, J.: Rapid increase in
- dichloromethane emissions from China inferred through atmospheric
- observations, Nat. Commun., 12(1), 7279,
- https://doi.org/10.1038/s41467-021-27592-y, 2021.
- Du, Y., Feng, M., Xu, Z., Yin, B., and Hobday, A. J.: Summer marine heatwaves in the
- 141 Kuroshio-Oyashio Extension region, Remote Sens., 14(13), 2980,
- https://doi.org/10.3390/rs14132980, 2022.
- Miller, B. R., Weiss, R. F., Salameh, P. K., Tanhua, T., Greally, B. R., Mühle, J., and
- Simmonds, P. G.: Medusa: A sample preconcentration and GC/MS detector
- system for in situ measurements of atmospheric trace halocarbons, hydrocarbons,
- 146 and sulfur compounds, Anal. Chem., 80(5), 1536–1545,
- 147 https://doi.org/10.1021/ac702084k, 2008.
- Nan, F., Yu, F., Xue, H., Wang, R., and Si, G.: Ocean salinity changes in the northwest
- Pacific subtropical gyre: The quasi-decadal oscillation and the freshening trend, J.
- 150 Geophys. Res.-Oceans, 120(3), 2179–2192,
- https://doi.org/10.1002/2014JC010536, 2015.
- Prinn, R. G., Weiss, R. F., Fraser, P. J., Simmonds, P. G., Cunnold, D. M., Alyea, F. N.,
- O'Doherty, S., Salameh, P., Miller, B. R., Huang, J., Wang, R. H. J., Hartley, D.
- E., Harth, C., Steele, L. P., Sturrock, G., Midgley, P. M., and McCulloch, A.: A
- history of chemically and radiatively important gases in air deduced from
- 156 ALE/GAGE/AGAGE, J. Geophys. Res.-Atmos., 105(D14), 17751–17792,
- https://doi.org/10.1029/2000JD900141, 2000.

- Roden, G. I.: Subarctic-subtropical transition zone of the North Pacific: Large-scale
- aspects and mesoscale structure, NOAA Tech. Rep. NMFS, 105(1), 1–38, 1991.
- US EPA: Method TO-15A: determination of volatile organic compounds (VOCs) in
- air collected in specially prepared canisters and analyzed by gas
- chromatography-mass spectrometry (GC-MS), United States Environmental
- Protection Agency, Washington, D.C., USA,
- https://nepis.epa.gov/Exe/ZyNET.exe/P100YDPO.TXT?ZyActionD=ZyDocume
- nt&Client=EPA&Index=2016+Thru+2020 (last access: 8 October 2025), 2019.
- 166 WMO (World Meteorological Organization): Scientific Assessment of Ozone
- Depletion: 2022, Global Ozone Research and Monitoring Project Report No.
- 278, World Meteorological Organization, Geneva, Switzerland, 509 pp., 2022.
- 169 Xu, F., Zhang, H. H., Yan, S. B., Sun, M. X., Wu, J. W., and Yang, G. P.:
- Biogeochemical controls on climatically active gases and atmospheric sulfate
- aerosols in the western Pacific, Environ. Res., 220, 115211,
- https://doi.org/10.1016/j.envres.2023.115211, 2023.
- 173 Yu, D., Yao, B., Lin, W., Vollmer, M. K., Ge, B., Zhang, G., Li, Y., Xu, H., O'Doherty,
- S., Chen, L., and Reimann, S.: Atmospheric CH₃CCl₃ observations in China:
- historical trends and implications, Atmos. Res., 231, 104658,
- https://doi.org/10.1016/j.atmosres.2019.104658, 2020.
- Zhang, G., Yao, B., Vollmer, M. K., Montzka, S. A., Mühle, J., Weiss, R. F.,
- O'Doherty, S., Li, Y., Fang, S., and Reimann, S.: Ambient mixing ratios of
- atmospheric halogenated compounds at five background stations in China,
- 180 Atmos. Environ., 160, 55–69, https://doi.org/10.1016/j.atmosenv.2017.04.017,
- 181 2017.